



Citation for published version:

Senthil, K, Sethi, M & Pelecanos, L 2023, 'Techniques to safeguard the underground tunnels against surface blast load', *International Journal of Critical Infrastructures*, vol. 19, no. 4, pp. 301-322.
<https://doi.org/10.1504/IJCIS.2023.132212>

DOI:

[10.1504/IJCIS.2023.132212](https://doi.org/10.1504/IJCIS.2023.132212)

Publication date:

2023

Document Version

Peer reviewed version

[Link to publication](#)

Copyright © 2023 Inderscience Enterprises Ltd. The final publication is available at International Journal of Critical Infrastructures via <https://www.inderscienceonline.com/doi/epdf/10.1504/IJCIS.2023.132212>

University of Bath

Alternative formats

If you require this document in an alternative format, please contact:
openaccess@bath.ac.uk

General rights

Copyright and moral rights for the publications made accessible in the public portal are retained by the authors and/or other copyright owners and it is a condition of accessing publications that users recognise and abide by the legal requirements associated with these rights.

Take down policy

If you believe that this document breaches copyright please contact us providing details, and we will remove access to the work immediately and investigate your claim.

Techniques to safeguard the Underground Tunnels against Surface Blast load

^aK. Senthil, ^aM. Sethi, ^bL. Pelecanos

^aDepartment of Civil Engineering, Dr. BR Ambedkar NIT Jalandhar, Punjab 144011, India

^bDepartment of Architecture and Civil Engineering, University of Bath, Bath, UK.

Abstract

Due to the growth of underground tunnels, the safety of structures under blast loading is a major threat. Therefore, this paper focused on various techniques such as tunnel burial depth, tunnel shape, tunnel lining materials and varying the location of the blast source to safeguard underground tunnels against blast load using numerical analysis. The behavior of concrete, reinforcement steel and the soil were incorporated by using the different constitutive model available in ABAQUS v. 2020. The predicted results were compared with the experimental results available in literature and found in close agreement. It is concluded that the layering of soil filling and depth of the burial of the tunnel found to be most important in case of external blast, whereas the stress bearing capacity of the concrete found to be important in case of internal blast. It is also concluded that the circular shape tunnel is one of the best performing tunnels.

Keywords: Tunnels, Blast Load, Burial depth, Lining Materials, Tunnel Shape, Blast Location

1. Introduction

The use of underground tunnels is getting common for various purposes to satisfy the demands of increasing population. The underground tunnels are being used for the transportation of various goods and commodities as well as for the movement of people from one place to another. With increasing use and popularity, the underground tunnels are always prone to the attacks by the enemies or natural calamities. Hence it is very important to predict and evaluate the damage being caused to the underground tunnels, as an effect of blast loading. Zhao et al. (2010) proposed a simple method for designing of concrete lining in tunnels subjected to explosive detonation on ground surface or explosion of a projectile penetrating into the ground located adjacent to the tunnel. The proposed method comprises of shotcrete/rockbolt support system, based on the single degree of freedom approach, which prevents the occurrence of spalling due to blast loads. The method follows a step by step procedure and avoid the usage of complex numerical calculations. Yang et al. (2010) studied

35 the dynamic behavior of circular metro tunnel against surface detonation. It was observed that
36 the upper part is considered the most vulnerable in comparison to other parts of the tunnel
37 against the detonation. Also, it was concluded that, if a surface explosion contains less than
38 500 Kg of TNT, then a lining thickness equal to 350 mm is considered the safe for depths more
39 than 7m.

40 **Xia et al. (2013)** predicted the amount of damage to rocks and the reinforced shotcrete
41 lining structure by the influence of an adjacent excavation blasting, in Damaoshan highway
42 tunnel. It was observed that for the peak particle velocity less than 0.3 m/s, no failure occurred
43 in the existing tunnel and at the rocks-lining interface. **Mobaraki and Vaghefi (2015)**
44 investigated the effect of surface explosion on Kobe box shaped tunnel and compared the
45 results with that of semi ellipse, horse shoe shaped and circular tunnel. It was observed that
46 circular and horseshoe shaped tunnels show less resistance to demolition than box shaped
47 tunnel, however the semi ellipse tunnel shows more resistance than box shaped tunnel. **Yu et**
48 **al. (2015)** investigated on square and circular shape's tunnel responses against internal
49 explosion. It was observed that the maximum effective plastic strain response at the critical
50 points (i.e. at the structural corner of tunnel and center of top plate) of square tunnel are
51 significantly lower as compared to the circular tunnel. **Tiwari et al. (2016)** studied the damage
52 caused to RC lining as well as the rocks surrounding the tunnel subjected to internal blast
53 loading. It was observed that the rocks surrounding the tunnel experience higher stress due to
54 damage in RC lining. Higher attenuation of shock wave is shown by the rocks having high
55 weathering conditions and low modulus. **Gao et al. (2016)** observed a decrease in dynamic
56 responses shown by cylindrical tunnels in an oscillating manner, when the time elapses.
57 However, these responses attenuate exponentially by increasing the distance between the
58 explosion source and the tunnel.

59 **Khan et al. (2016)** studied the tunnels made up of cast iron lining and subjected to
60 internal blast loading. The blast response of tunnels was found affected significantly by tunnel
61 lining thickness, peak blast pressure and soil and rock elastic moduli. The corresponding results
62 were found less affected by soil and rock dilation angle. It was recommended that in order to
63 create a blast resistant tunnel design, an increase in the lining thickness shall be viable option.
64 **Dang et al. (2018)** studied the damage caused to the concrete lining of an existing tunnel, due
65 to the blasting activities used for the construction of a new adjacent tunnel. It was observed
66 that the tunnel side facing the blast source undergoes greater damage as compared to the face
67 of tunnel away from the blast source. It was concluded that, more is the distance between the
68 blast source and the existing tunnel face, more is the safety of the concrete lining in the existing

69 tunnel. **Hu et al. (2018)** proposed a model to study the vibration response shown by concrete
70 segmental tunnel lining against internal blast loading acting axisymmetrically. During the
71 expansion deformation process, stiffness of the joint bolt plays an essential role. For the case
72 of contraction phase, all the compression effect is taken by the concrete segments. **Majumder
73 and Bhattacharya (2019)** studied the performance of intermittent geofam infilled trench as
74 a passive vibration screening method for a reinforced concrete lining tunnel subjected to
75 internal blast loading. It was concluded that the trench installed with passive vibration
76 screening technique shall help in the reduction of blast waves causing ground vibrations.

77 **Ambrosini and Luccioni(2019)** studied about the propagation of shock waves in the soil
78 and the main phenomenon taken under consideration were formation of shock waves,
79 propagation of elastic plastic wave in the soil and interaction between soil and structures. It
80 was observed that the properties of soil play a major role to determine the propagation of shock
81 waves in the soil. However, the soil properties have an insignificant effect on the diameter of
82 the crater. **Bettelini (2019)** proposed a holistic approach to ensure the safety in underground
83 tunnel networks against risks generated by natural phenomenon (eg- gas radiation, temperature
84 rise, lack of oxygen) or human activities (eg- smoke, fire, terrorist explosions or structure
85 failure). It was observed that the safety proposals comprised providing safety barriers against
86 hazards and multiple protection layers to reduce the harm generated by hazards. **Vinod and
87 Khabbaz (2019)** compared the surface settlements and moments generated while boring of
88 circular and rectangular twin tunnels in weak ground. It was observed that, for weak grounds
89 and shallow depths, rectangular tunnels show lesser settlements in comparison to circular
90 tunnels. However, higher bending moments are produced in rectangular tunnels compared to
91 circular tunnels. **Prasanna and Boominathan (2020)** observed lesser damage in cast iron
92 tunnels as compared to RCC tunnels subjected to internal blast loading. The reason may be due
93 to the higher stiffness and density is possessed by cast iron tunnels than RCC tunnels. **Jagriti
94 Mandal et al. (2020)** found that 10% decrease in peak displacement in case of circular cross
95 section tunnel and it may be due to less reflected pressure waves were generated on circular
96 surface compared to box shaped and horseshoe shape tunnel. **Liu et al. (2020)** considered the
97 effect of blast load used for the construction of a new tunnel adjacent to an existing circular
98 highway tunnel named Huanglongshan. The peak particle velocity of the lining structure
99 present in the existing tunnel was studied. It was observed that the peak particle velocity value
100 was higher at the face located in front of the blast source as compared to the face placed behind
101 the blast source. **Goel et al. (2020)** carried out finite element analysis for comparison of the
102 damage caused to the tunnel and surrounding soil considering three different tunnel cross

103 sections i.e. arched, circular and rectangular using 100 Kg TNT explosive for saturated and
104 unsaturated soil conditions. It was observed that arched as well as rectangular lining
105 experienced 29.56% and 50.31% more displacement compared to the circular lining on the top
106 node of the tunnel lining without any change in other parameters. **Ata et al. (2021)** studied the
107 effect of blast loading by considering the mass of TNT as 100, 200, 300 and 400 Kg. An
108 increase of 64% of kinetic energy was observed when the charge weight was increased from
109 100 to 400 Kg. **Mandal et al. (2021)** observed an increase in the displacement at tunnel roof
110 center by 94 and 324% by increasing the charge weight from 250 to 500 Kg and 1000 Kg
111 respectively.

112 **Zhang et al. (2021)** proposed a study based on andesitic porphyrite failure rule adopted
113 by the technique of open cut blasting in reservoir tunnel. It was observed by test results as well
114 as the numerical analysis that, blasting excavation through andesitic porphyrite proved to be
115 suitable for just 1-2 areas.

116 Based on the detailed literature review, it was observed that the investigations on the
117 evaluation of mitigation strategies on tunnels against surface blast loading are limited. Also,
118 the studies revealed that the influence of tunnel burial depth, influence of tunnel shapes and
119 influence of different tunnel lining materials subjected to external surface blast loading are
120 found to be limited. Therefore, this paper is focused on the prediction of mitigation strategies
121 of underground tunnels against surface blast loading using finite element technique, ABAQUS
122 Explicit software v. 2020. The concrete, reinforcement steel and the soil were modelled and
123 the constitutive behavior was incorporated using the model such as Concrete Damage Plasticity
124 Model, Johnson Cook Model and Drucker Prager model respectively, see **Section 2** and
125 **Section 3**. The results in terms of acceleration thus predicted were compared with the
126 experimental results available in the literature, see **Section 4**. Further, the simulations were
127 conducted by varying tunnel burial depth, tunnel shape, tunnel lining materials and varying the
128 location of the blast source in order to estimate the mitigation strategies of the underground
129 tunnels, see **Section 5**.

130

131 **2. Constitutive Modelling**

132 The constitutive model and the material behaviour such as concrete, metals and soil are
133 discussed in this Section. The inelastic behaviour of concrete was modelled by using Concrete
134 Damage Plasticity model, available in ABAQUS/Explicit. The Johnson-Cook model was used
135 to incorporate the elastic and plastic behaviour of steel reinforcement bars as well as lining

136 materials of aluminium alloy. The Drucker Prager model was used to model the soil elements
137 are discussed here.

138

139 **2.1 Johnson-Cook model for Aluminium and Steel Reinforcement**

140 Johnson-Cook elasto- viscoplastic material model, available in ABAQUS/Explicit v.
141 2020 is used to predict the flow and fracture behaviour of aluminium alloy and steel
142 reinforcement bars. The model is based on the criteria of associated flow rule and von Mises
143 yield criterion. The effects of thermo-elasticity, plastic flow, yielding, isotropic strain
144 hardening, strain rate hardening, softening due to adiabatic heating and damage are included
145 in this model. Various constants are used to define the Johnson Cook model, which comprises
146 of initial yield of the material, strain hardening coefficient, strain hardening exponent, strain
147 rate sensitivity and thermal softening parameter, denoted by A, B, C and m respectively. The
148 Johnson-cook material parameters for aluminium as well as steel reinforcement are given in
149 **Table 1**. This model can also be used along with some damage and failure models, due to the
150 provision of which certain damage initiation criteria can be specified. Further, a smooth
151 degradation of the material can be supported by the progressive damage models, hence making
152 the materials suited for dynamic and quasi-static situations. The elements possessing
153 displacement degree of freedom as available in ABAQUS software can support the use of
154 Johnson-Cook model.

155

156 **2.2 Concrete Damaged Plasticity Model for Concrete**

157 The inelastic behaviour of concrete is modelled by using concrete damaged plasticity
158 model, which incorporates both tensile and compressive behaviour of concrete. This model can
159 appropriately define the inelastic behaviour of concrete, based on the concept of elastic damage
160 in combination with isotropic expansion and compression flexibility. This model can be used
161 to define the behaviour of both reinforced concrete as well as plain concrete. This model can
162 be used to define the concrete behaviour, also with that of the presence of rebars to define
163 reinforced concrete. This model may help to define the behaviour of concrete, subjected to
164 monotonic cyclic or dynamic loading conditions under low confining pressures. The model can
165 also be defined, being sensitive to the strain rate. The two main failure mechanisms, including
166 tensile cracking and compressive crushing of the concrete material are assumed by this model.
167 Two hardening variables namely ε_c^{pl} and ε_t^{pl} which are compressive and tensile equivalent
168 plastic strains, respectively control the evolution of the yield surface and are linked to failure
169 mechanisms under tension and compression loading. The damage variable values can vary

170 from zero to one, where zero represents the undamaged material and one represents total loss
171 of strength. This model works on the principle of isotropic and linear damage of concrete,
172 which is subjected to arbitrary loading conditions. The stress strain relations under uniaxial
173 compression and tension loading are given by the following equations where E_o is the initial
174 (undamaged) elastic stiffness of the material: $\sigma_t = (1-d_t)E_o(\varepsilon_t - \varepsilon_t^{pl})$ and $\sigma_c = (1-d_c)E_o(\varepsilon_c - \varepsilon_c^{pl})$,
175 where d_t and d_c are tension damage variable and compression damage variable respectively.
176 The concrete damaged plasticity model parameters for concrete are given in **Table 2-6**.

177

178 2.3 Drucker-Prager model for soil

179 Drucker-Prager model is the simplification of Mohr-Coulomb model, where the
180 hexagonal shaped failure cone was replaced by a simple cone. The circular yield is possessed
181 by the Drucker-Prager model, which is equidistant from the center to the yield surface. The
182 yield area in this model consists of two main areas i.e. the fracture area providing the flow cut
183 and the cover, crossing the equivalent pressure. This model is based on Drucker Prager yield
184 criteria, which is used to detect if a particular material has undergone plastic yielding or not.
185 The Drucker-Prager shear criterion is considered as linear and Drucker-Prager hardening
186 behaviour was defined as compression, having yield stress versus absolute plastic strain. The
187 Drucker-Prager material parameters for the considered soil are given in **Table 7**. The cohesive
188 behavior such as normal stiffness, shear stiffness and tensile strength were taken as 315, 82
189 and 1 MPa respectively, which is defined as a contact property between tunnel and soil.

190

191 3. Finite Element Modelling

192 The modelling of the concrete, soil, reinforcement as well as acoustic infinite element
193 was carried out using ABAQUS/CAE v.2020. A 0.8 x 0.8 m internal clear square was
194 considered as the size of tunnel, taken exactly similar to the tunnel size as proposed by **Soheyli**
195 **et al., (2016)**, see **Fig 1**. The length, width and height of the model was considered as 12.0, 4.0
196 and 4.5 m respectively. The thickness of the tunnel lining was considered as 100 mm. A cover
197 of 50 mm was provided on both sides of the tunnel wall. The geometry of soil, concrete and
198 steel reinforcement bars were modelled as solid deformable bodies, **Fig 1(a)-(d)**. The tie
199 constraint option available in ABAQUS/CAE was used to provide interaction between concrete
200 and steel, wherein concrete was considered as the host region and the steel was considered as
201 embedded region. The Concrete Damaged Plasticity model and Johnson-Cook model
202 parameters were defined to incorporate the constitutive behaviour of concrete and steel
203 reinforcement. The origin of blast produced by 1.69Kg TNT mass was considered by using

204 CONWEP model with AIR BLAST definition available in ABAQUS/CAE v.2020. A single
205 layer of main as well as transverse reinforcement were provided with 8mm diameter bars, with
206 100 mm center to center spacing, see **Fig 1(a) and Fig 1(c)**. The strength and failure properties
207 of the steel reinforcement were provided as proposed by **Borvik et al. (2001)**, providing a steel
208 section of 460 MPa, however the yield strength of steel reinforcement was 340 MPa, as taken
209 by **Soheyli et al. (2016)**. The acoustic infinite element was considered as an acoustic medium
210 with bulk density of 1500 Kg/m^3 and density of 110 Kg/m^3 , to define the exterior boundary of
211 the soil strata. **ACIN3D4** elements were used in the present study to define the acoustic infinite
212 elements, that are used to define the outer boundary of the model to remove the requirement of
213 impedance type absorbing boundary conditions. A fake contact has been defined between the
214 soil outer surface and the acoustic infinite medium. The connection between the tunnel outer
215 surface and the soil was provided through a surface to surface contact between the two,
216 considering tunnel as the master surface and the surrounding soil as the slave surface. The
217 results thus obtained were compared with that of experimental results as proposed by **Soheyli**
218 **et al., (2016)**.

219 A detailed mesh convergence study has been conducted, to study the effect of varying
220 mesh size of the tunnel, under consideration on its behaviour towards the blast waves. The
221 mesh size of the tunnel was varied to 50 mm, 40 mm, 30 mm and 20 mm. Total number of
222 elements were 11520, 26800, 63973 and 191400 for the case of 50, 40, 30 and 20 mm mesh
223 size of the concrete tunnel, respectively. The results were recorded in terms of acceleration and
224 von-Mises stresses in the concrete tunnel for varying mesh sizes, as shown in **Fig 2** and **Fig 3**.
225 It has been observed from **Fig 2(a-d)**, that the acceleration value for various mesh sizes is
226 almost same i.e. 2.97 g. The variation of von-Mises stress values for various mesh sizes has
227 been shown in **Fig 3(a-d)**. From the mesh convergence study, it can be concluded that 50 mm
228 mesh size is most suitable from computational cost point of view. Hence, 50 mm mesh size
229 can be used for further analysis. The total number of linear hexahedral element of C3D8R were
230 402888, linear line element type T3D2 were 28080, linear quadrilateral elements of type
231 ACIN3D4 were 1918, quadratic tetrahedral elements of type C3D10M were 5735 and the total
232 number of elements for the standard simulations were 438621.

233

234

235 4. Validation of Finite Element Results

236 The simulations were carried out against 1.69 Kg TNT mass, placed at a distance of 4m
237 from the surface of the front wall. The constitutive modelling of the steel reinforcement and

238 the concrete was done by using Johnson-cook model and Concrete Damaged Plasticity model
239 respectively. The Drucker-Prager model has been used to predict the behaviour of the soil, see
240 **section 2**. The use of acoustic infinite elements was employed in order to remove the
241 requirement of impedance- type absorbing boundary conditions on the outer boundary. The
242 finite element modelling of the soil element, along with the RCC tunnel has been explained in
243 **Section 3**. The simulation results, thus obtained were compared with the experimental results
244 as given by **Soheyli et al., (2016)**. **Fig 4** shows the comparison between the actual and the
245 predicted acceleration of the tunnel. The acceleration in the tunnel was noted at the node which
246 was closest to the point of observation, taken in the actual experimental work. The numerical
247 results predicted the pattern of acceleration almost accurately, in the given time step. A good
248 agreement was observed between the acceleration values obtained from the simulation results
249 as well as the experimental results. In general, a maximum deviation of 20% was observed
250 between the actual and the predicted acceleration values of the tunnel. **The simulation shows**
251 **good agreement with the experimental measurements at the final stage, for $t \geq 0.05$ sec.**
252 **However, at the early stage where $t < 0.05$ sec, it seems that the maximum deviation between**
253 **the experimental and numerical results is more than 20%, especially in the second and third**
254 **acceleration peaks. The reason may be due to the fact that the deviation between the parameters**
255 **of steel reinforcement bars considered in the model and experiment. Moreover, exact**
256 **parameters for the soil surrounding the tunnel were missing from the literature. Due to the**
257 **variation between the different parameters used, there is a deviation between the experimental**
258 **and simulation results.** Hence, it was concluded that the present study successfully
259 demonstrates the accuracy of the finite element models of the tunnel.

260

261 **5. Evaluation of Mitigation Strategies**

262 The simulations were performed on important parameters such as influence of the
263 location of blast, influence of tunnel burial depth, influence of tunnel shapes and influence of
264 varying tunnel lining materials, in order to establish the mitigation strategies of underground
265 tunnels against external surface blast loading. The response of the tunnels was presented in
266 terms of acceleration and von-Mises stresses and the same is discussed in this section.

267

268 **5.1 Influence of Location of the Blast Source**

269 The simulations were carried out on a 4 m long Square Box shaped tunnel with 0.8x0.8
270 m clear square cross section and 100 mm thick tunnel lining, subjected to a blast load produced
271 by 1.69 Kg TNT, by placing the blast source at three different locations i.e. externally within

272 the soil strata at a distance of 4 m horizontally away from the tunnel front wall, internally at
273 the centre of the tunnel (internal blast), and surface blast at a distance of 0.25 m from the top
274 surface of the soil element, for total time period of 0.12 second. The tunnels were buried at a
275 depth of 1 m from the natural ground surface. The acceleration on the inner face of the tunnel
276 front wall against blast load of 1.69 Kg, for three different positions of the blast source, are
277 shown in **Fig 5**. The maximum acceleration was found to be 2337.3 g for the case of internal
278 blast loading, followed by 36.48 g for surface blast loading and 2.97 g for external blast
279 loading. It was also observed that the acceleration reaches its peak within 0.0288 sec from the
280 time of detonation for the case of internal blast loading. However, the peak acceleration was
281 found at 0.0096 and 0.0276 sec for the case of surface blast loading and external blast loading,
282 respectively. The reason for 0.0288 sec from detonation by internal blast loading may be due
283 to the fact that the peak acceleration caused by the reflected waves, whereas the peak
284 acceleration was caused by direct waves at 0.0096 and 0.0276 sec in case of surface blast and
285 external blast loading respectively.

286 The von-Mises stresses in concrete against blast load of 1.69 kg mass of TNT for different
287 blast positions is shown in **Fig 6**. In case of internal blast loading, the stresses in concrete were
288 found to be 8.09, 10.17 and 9.358 MPa at 0.024, 0.036 and 0.048 Sec respectively. For surface
289 blast loading, the stresses in concrete was 4.24, 4.35 and 4.38 MPa at 0.024, 0.036 and 0.048
290 Sec respectively. Similarly, for external blast loading, the stresses in concrete were 1.31, 0.20
291 and 0.14 MPa at 0.024, 0.036 and 0.048 sec respectively. It is observed that the stress in the
292 chosen concrete tunnel was found to be in the range of 10.17-0.14 MPa and however the **stress**
293 **bearing capacity** of the concrete is quite high, i.e. 20 MPa. It is concluded that the strength of
294 concrete is more important in case of tunnel against internal blast loading.

295 The von-Mises stresses in soil element surrounding the tunnel against blast load of 1.69
296 kg mass of TNT for different blast positions is shown in **Fig 7**. In case of internal blast loading,
297 the stresses in soil element was found to be 0.59, 0.24 and 0.11 MPa at 0.0012, 0.0036 and
298 0.006 Sec respectively. For surface blast loading, the stresses in soil element were 2.06, 0.44
299 and 0.27 MPa at 0.0012, 0.0036 and 0.006 Sec respectively. Similarly, for external blast
300 loading, the stresses in soil element were 1.05, 0.55 and 0.25 MPa at 0.0012, 0.0036 and 0.006
301 sec respectively. It is observed that the sensitivity on soil against surface blast loading is
302 significant. Therefore, it is concluded that the layering of soil filling or depth of the burial of
303 tunnel are more important in case of tunnel against surface blast loading as well as external
304 blast loading.

305

306 5.2 Influence of Tunnel Burial Depth

307 In order to study the influence of burial depth of reinforced concrete tunnel, the
308 simulations on varying tunnel burial depth such as 1, 2 and 3 m were modelled against 1.69 kg
309 mass of TNT placed at a distance of 0.25 m from the top surface of the soil for total time period
310 of 0.12 second, see Fig 8. The acceleration on the inner face of the front wall RCC concrete
311 square tunnels at burial depth of 1, 2 and 3 m against surface blast load is shown in Fig 9. The
312 maximum acceleration was found to be 36.48, 6.22 and 1.5 g against 1, 2 and 3 m tunnel burial
313 depth respectively. It was observed that the burial depth of the tunnel is significantly reducing
314 the acceleration in the tunnel. It was also clearly seen that the acceleration reaches its peak
315 value within 0.0096 sec from the time of detonation in case of burial depth of 1 m. However,
316 the peak acceleration was observed at 0.0156 and 0.0312 seconds in case of burial depth of 2
317 and 3 m respectively.

318 The von-Mises stresses in the tunnel at varying tunnel burial depth against surface blast
319 load is shown in Fig 10 a(i)-(iii). At 1 m tunnel burial depth, the stresses in concrete were
320 4.24, 4.35 and 4.38 MPa at 0.024, 0.036 and 0.048 Sec respectively. In case of 2 m tunnel
321 burial depth, the stresses in concrete were 2.25, 2.15 and 2.59 MPa at 0.024, 0.036 and 0.048
322 Sec respectively. Similarly, the stresses were found in concrete i.e., 0.72, 0.30 and 0.09 MPa
323 at 0.024, 0.036 and 0.048 Sec respectively at 3 m tunnel burial depth. Overall, it is observed
324 that the stress in concrete was found to be in the range of 4.38 to 0.09 MPa for the chosen mass
325 of TNT. Therefore, it is concluded that the burial depth of the tunnel is one of the important
326 parameter which affects the function of the tunnel against surface blast loading.

327

328 5.3 Influence of varying tunnel shapes

329 In order to evaluate the efficiency of the shape of the reinforced concrete tunnel. the
330 square box shape, semi-circular and circular tunnel were modelled against 1.69Kg mass of
331 TNT, placed at a distance of 0.25 m from the top surface of soil for total time period of 0.12
332 second, see Fig 11. The acceleration on the inner face of the tunnel front wall of different tunnel
333 shapes is shown in Fig 12. The maximum acceleration was found to be 36.48 g for square box
334 shaped tunnel, followed by 16.73g for circular tunnel and 9.56g for semi-circular tunnel. It was
335 also observed that the acceleration reaches its peak within 0.0096 seconds from the time of
336 detonation in case of square box shaped tunnel. However, the peak acceleration was observed
337 at 0.0096 and 0.018 sec in case of semi-circular tunnel and circular tunnel.

338 The von-Mises stresses in reinforced cement concrete of different tunnel shapes against
339 blast load is shown in Fig 13(a-i)-(c-iii). In case of square tunnel, the stresses in concrete were

340 found to be 4.24, 4.35 and 4.38 MPa at 0.024, 0.036 and 0.048 Sec respectively. In semi-
341 circular tunnel, the stresses in concrete were 2.27, 2.42 and 2.67 MPa at 0.024, 0.036 and 0.048
342 Sec respectively. Similarly, for circular tunnel, the stresses in concrete were 2.20, 2.89 and
343 3.32 MPa at 0.024, 0.036 and 0.048 Sec respectively. However, it was observed that the stress
344 in the chosen concrete tunnel was found to be in the range of 4.38-2.20 MPa. Among the chosen
345 cases, the circular tunnel offers better performance followed by the semi-circular and square
346 tunnel. The reason for better performance of circular tunnel is may be due to the curvature in
347 nature of tunnel. Therefore, it is concluded that the circular tunnel is one of the best performing
348 tunnel against surface blast loading, among the chosen cases.

349

350 **5.4 Influence of Tunnel lining materials**

351 The simulations were carried on Reinforced Concrete (RCC), Plain Concrete (PC) and
352 Aluminium lined tunnels against 1.69 Kg mass of TNT, placed at a distance of 0.25 m from
353 the top surface of surrounding soil element of the tunnel, **for total time period of 0.12 second.**
354 The thickness of RCC, PC and aluminium lining was 100mm. The acceleration on the inner
355 face of the tunnel front wall with different lining materials against blast load is shown in **Fig**
356 **14.** The maximum acceleration was found to be 596.1 g for PC, followed by 36.4g for RCC
357 and 16.81g for aluminium. It is also observed that the acceleration reaches its peak value within
358 0.01092, 0.0096 and 0.0072 seconds from the time of detonation in case of PC, RCC and
359 Aluminium tunnels, respectively. It is concluded that plain concrete is least performing
360 material against blast loading among the chosen cases.

361 The von-Mises stresses in tunnel having different lining materials against blast load of is
362 shown in **Fig 15 (a-i)-(c-iv).** In case of PC tunnel, the Mises stresses in tunnel was 3.42, 3.51
363 and 3.56 MPa at 0.024, 0.036 and 0.048 Sec respectively. In RCC tunnel, the stresses in
364 concrete were 4.24, 4.35 and 4.38 MPa at 0.024, 0.036 and 0.048 Sec respectively. In
365 Aluminium tunnel, the stresses in lining was 1.74, 1.99 and 1.61 MPa at 0.024, 0.036 and 0.048
366 Sec respectively. However, it was observed that the stress in aluminium tunnel was found to
367 significantly less as compare to PC and RCC. The reason may be due to the fact that the blast
368 resistance capacity of aluminium is significantly higher as compared to other materials.

369

370 **6. CONCLUSIONS**

371 This paper is focused on the prediction of mitigation strategies of underground tunnels
372 against surface blast loading using finite element technique. **The present study has focused to**
373 **present the best possible measures to safeguard the underground tunnels against the effects of**

374 blast waves. The mitigation of the tunnel damage against surface blast loading has been
375 proposed by providing suitable tunnel lining materials, tunnel burial depth and tunnel shapes.
376 Also, the variation in the tunnel damage intensity through different positions of the blast source,
377 are also discussed in this study.

378 The simulations were conducted on the underground tunnels against surface blast loading
379 studied considering the different location of blast, influence of tunnel burial depth,
380 influence of tunnel shapes and influence of varying tunnel lining materials. The response
381 of the tunnel was studied in terms of acceleration and Mises stresses and following
382 conclusions were drawn;

- 383 • It was observed that the acceleration and von-Mises stress in the tunnel is significantly
384 higher for the case of internal blast loading as compared to the case of external blast
385 loading and surface blast loading. It is concluded that the layering of soil filling or depth
386 of the burial of tunnel are more important in case of tunnel against surface blast loading
387 as well as external blast loading, however, the **stress bearing capacity** of the concrete is
388 important in case of internal blast loading.
- 389 • It is concluded that the burial depth of the tunnel is one of the important parameter which
390 affects the function of the tunnel against surface blast loading. Hence, more is the burial
391 depth of the tunnel, lesser damage would be caused to the tunnel against surface blast
392 loading.
- 393 • It is concluded that the circular tunnel is one of the best performing tunnel against surface
394 blast loading, among the chosen cases. Also, it was observed that the square shape tunnel
395 experience the highest acceleration and Mises stress. Hence this shape of the tunnel is
396 most vulnerable against surface blast loading as compared to circular and semi-circular
397 shape tunnel.
- 398 • It is concluded that plain concrete is least performing material against blast loading
399 among the chosen cases. The aluminium lined tunnel seems to be the best suitable tunnel
400 lining material among the chosen cases, as the acceleration and von-Mises stress is
401 minimum.

402

403 REFERENCES

- 404 1. ABAQUS/CAE User's Manual, SIMULIA. Version 6.14.
- 405 2. Ambrosini, D., Luccioni, B. (2019). Effects of underground explosions on soil and
406 structures. *Underground Space Journal*, 5.

- 407 3. Ata A, Nabil M, Hassan S, Nawar M. (2021;). Numerical analysis of underground
408 tunnels subjected to surface blast loads. *Frat ed Integrita Strutt.* 15(55):159–73.
- 409 4. Bettelini, M. (2019). Systems Approach to Underground Safety. *Underground Space*
410 *Journal.* 5.
- 411 5. Borvik, T., Hopperstad, O.S., Berstad, T., Langseth, M. (2001) A computational model
412 of viscoplasticity and ductile damage for impact and penetration. *European Journal of*
413 *Mechanics and Solids* 20, 685–712.
- 414 6. Dang VK, Dias D, Do NA, Vo TH.(2018) Impact of blasting at tunnel face on an
415 existing adjacent tunnel. *International Journal of GEOMATE.*15(47):22–31.
- 416 7. Gao M, Zhang JY, Chen QS, Gao GY, Yang J, Li DY.(2016) An exact solution for
417 three-dimensional (3D) dynamic response of a cylindrical lined tunnel in saturated soil
418 to an internal blast load. *Soil Dynamics and Earthquake Engineering.*90:32–7.
- 419 8. Goel, M.D., Verma, S. & Panchal, S. (2021) Effect of Internal Blast on Tunnel Lining
420 and Surrounding Soil. *Indian Geotechnical Journal* 51, 359–368.
- 421 9. Hu K, Vafeidis A, Chu C, Zhao Y.(2018) Vibration of a segment tunnel lining under
422 internal blast loading. *Journal of Vibroengineering.*20(1):448–58.
- 423 10. Khan S, Chakraborty T, Matsagar V.(2016) Parametric Sensitivity Analysis and
424 Uncertainty Quantification for Cast Iron–Lined Tunnels Embedded in Soil and Rock
425 under Internal Blast Loading. *Journal of Performance of Constructed Facilities.*
426 30(6):04016062.
- 427 11. Liu Z, Jiang N, Sun J, Xia Y, Lyu G. (2020;). Influence of tunnel blasting construction
428 on adjacent highway tunnel: A case study in Wuhan, China. *International Journal of*
429 *Protective Structures.* 11(3):283–303.
- 430 12. Majumder M, Bhattachryya S.(2019) An alternate arrangement of geofoam blocks and
431 air pocket to mitigate confined blast induced vibration. *International Journal of*
432 *Geotechnical Engineering.* 00(00):1–14.
- 433 13. Mandal J, Agarwal AK, Goel MD.(2020) Numerical Modeling of Shallow Buried
434 Tunnel Subject to Surface Blast Loading. *Journal of Performance and Construction*
435 *Facilities.*34(6):04020106.
- 436 14. Mandal J, Goel M, Agarwal A. (2021.). Numerical Modeling of Tunnel Subjected to
437 Surface Blast Loading. In: Saha SK, Mukherjee M (eds) *Recent Advances in*
438 *Computational Mechanics and Simulations Lecture Notes in Civil Engineering, vol 103*
439 *Springer, Singapore.*
- 440 15. Mobaraki B, Vaghefi M.(2015) Numerical study of the depth and cross-sectional shape

- 441 of tunnel under surface explosion. *Tunnelling and Underground Space Technology*.
442 47:114–22.
- 443 16. Prasanna R, Boominathan A.(2020) Finite-Element Studies on Factors Influencing the
444 Response of Underground Tunnels Subjected to Internal Explosion. *International*
445 *Journal of Geomechanics*. 20(7):04020089.
- 446 17. Senthil K., Iqbal, M.A., Arindam, B., Mittal, R., Gupta, N.K.. (2018). Ballistic
447 resistance of 2024 aluminium plates against hemispherical, sphere and blunt nose
448 projectiles. *Thin-Walled Structures*. 126. 94-105.
- 449 18. Senthil K., Pelecanos L., Rupali S., Prediction of damage intensity of reinforced
450 concrete tunnels and soil against blast loading, 10th International Symposium on
451 Geotechnical Aspects of Underground Construction in Soft Ground, University of
452 Cambridge, 29th June – 01st July 2020, UK (Postponed).
- 453 19. Senthil K., Sethi M., Pelecanos L., Mitigation Strategies of Underground Tunnels
454 against Blast Loading. *International Journal of Protective Structures*(Under Review).
- 455 20. Soheyli, M.R., Akhaveissy, A.H., Mirhosseini, S.M. (2016) Large-scale experimental
456 and numerical study of blast acceleration created by close-in buried explosion on
457 underground tunnel lining. *Shock and Vibration*. 2016, Article ID 8918050.
- 458 21. Tiwari R, Chakraborty T, Matsagar V.(2016) Dynamic Analysis of Tunnel in
459 Weathered Rock Subjected to Internal Blast Loading. *Rock Mechanics and Rock*
460 *Engineering*. 49(11):4441–58.
- 461 22. Vinod, M.,Khabbaz, H. (2019). Comparison Of Rectangular And Circular Bored Twin
462 Tunnels In Weak Ground. *Underground Space Journal*, 4.
- 463 23. Xia X, Li HB, Li JC, Liu B, Yu C.(2013) A case study on rock damage prediction and
464 control method for underground tunnels subjected to adjacent excavation blasting.
465 *Tunnelling and Underground Space Technology*.35:1–7.
- 466 24. Yang Y, Xie X, Wang R.(2010) Numerical simulation of dynamic response of
467 operating metro tunnel induced by ground explosion. *Journal of Rock Mechanics and*
468 *Geotechnical Engineering*.2(4):373–84.
- 469 25. Yu H, Wang Z, Yuan Y, Li W.(2015) Numerical analysis of internal blast effects on
470 underground tunnel in soils. *Structure and Infrastructure Engineering*. 12(9):1090–105.
- 471 26. Zhang GY, Xie W, Yang QG, Luo J. (2021) Research on open cut blasting technology
472 of reservoir diversion tunnel. *International Journal of Critical Infrastructures*.
473 2021;17(1):21-37.
- 474 27. Zhao PJ, Lok TS, Yin ZQ, Zhou ZL.(2010) Simplified design of rock cavern concrete

475 lining to resist shock loading. Journal of Central South University of
476 Technology.17:1087-1094.

477

478

479

480

481

482

483

484

485

486

487

488

489

490

491

492

493

494

495

496

497

498

499

500

501

502

503

504

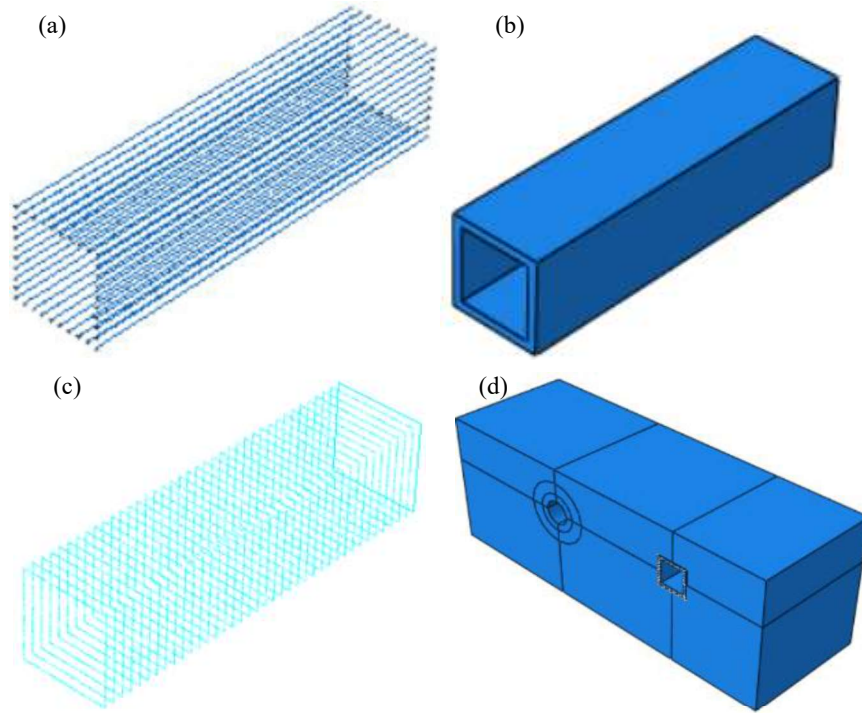
505

506

507

508

509



510

511

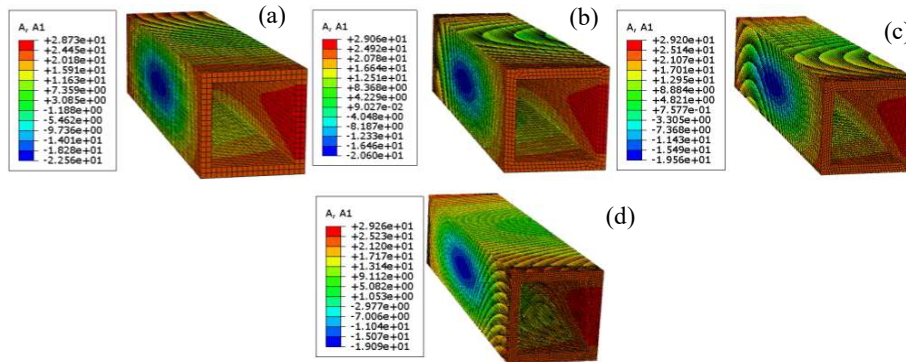
Fig 1. Tunnel (a) longitudinal reinforcement bar (b) concrete (c) transverse reinforcement bar (d) isometric view of combined finite element model

512

513

514

515



516

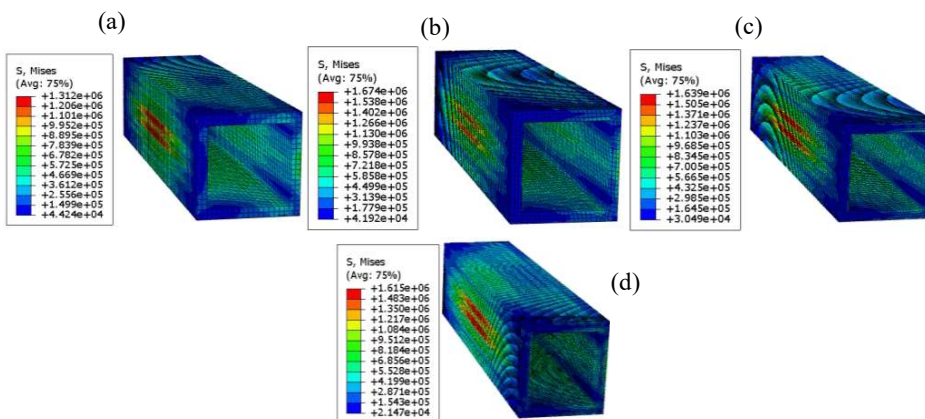
517

Fig 2. Acceleration in concrete tunnel at (a) 50mm (b) 40mm (c) 30mm and (d) 20 mm mesh size

518

519

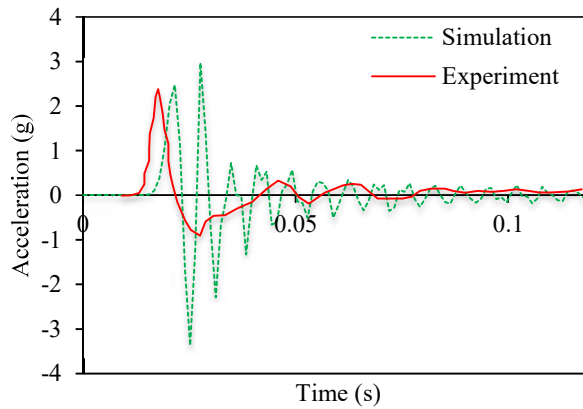
520



521

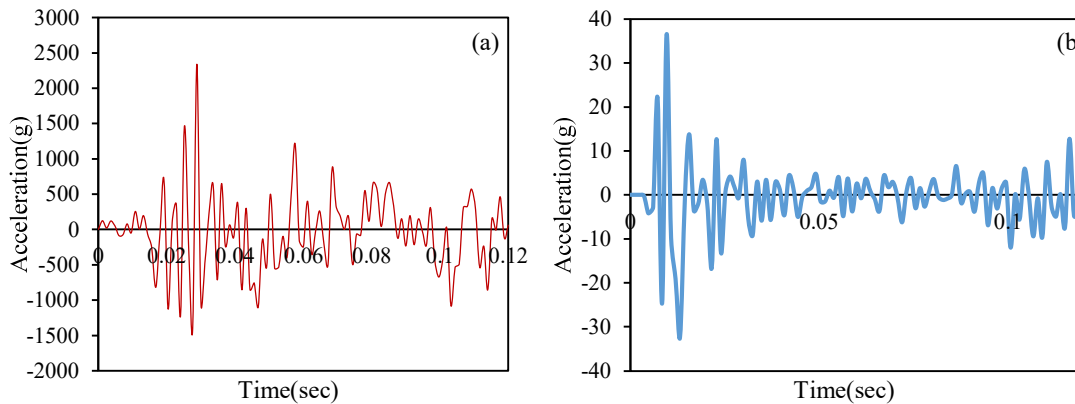
522 Fig 3. Mises stresses in concrete tunnel at (a) 50mm (b) 40mm (c) 30mm and (d) 20 mm
523 mesh size

524

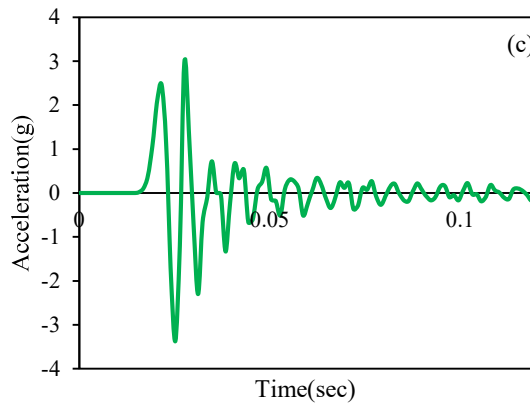


525 Fig 4. Comparison of acceleration obtained from simulation and experiment with 1.69 Kg
526 mass of TNT at a distance of 4 m from the tunnel front wall

527
528
529



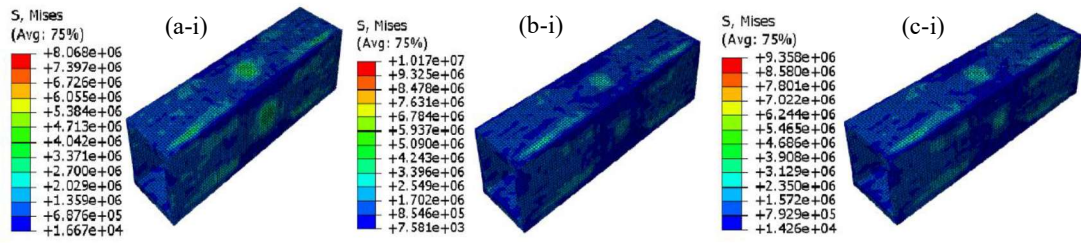
530



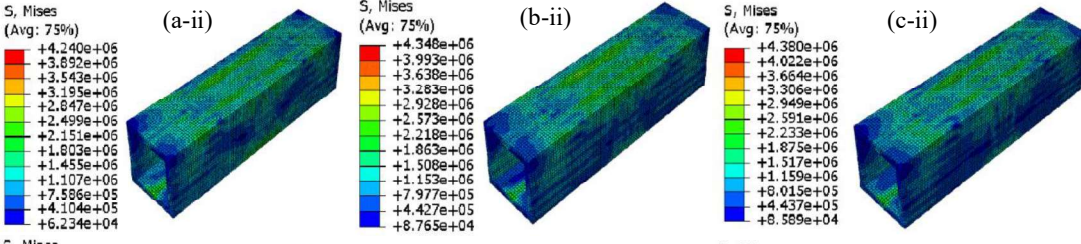
531 Fig 5. Acceleration function of time in the tunnel against (a) internal blast (b) surface blast
532 and (c) external blast loading

533
534
535

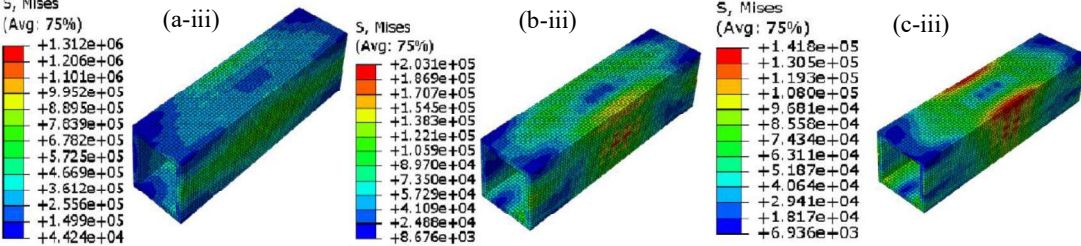
536



537



538



539

540

Fig 6. Mises stress in the tunnel front wall at (a) 0.024 (b) 0.036 and (c) 0.048 sec against (i) internal (ii) surface and (iii) external blast loading

541

542

543

544

545

546

547

548

549

550

551

552

553

554

555

556

557

558

559

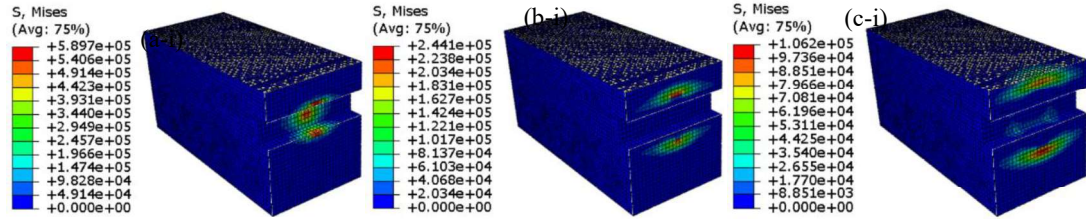
560

561

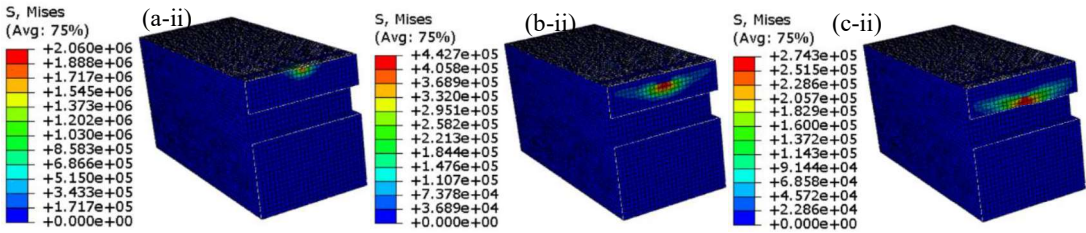
562

563

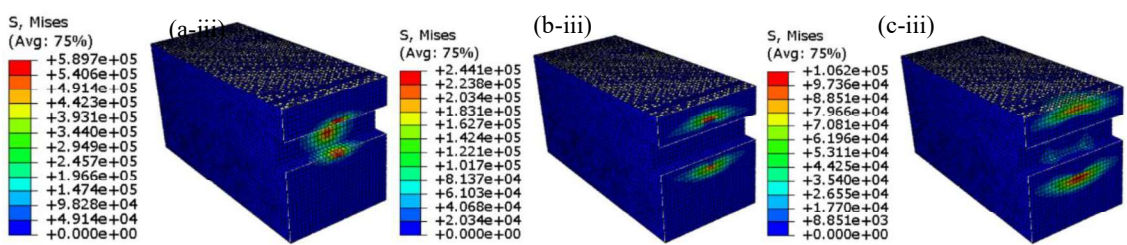
564



565



566



567

Fig 7. Mises stress in the tunnel front wall at (a) 0.0012 (b) 0.0036 and (c) 0.006 sec for (i)

568

internal (ii) surface and (iii) external blast loading

569

570

571

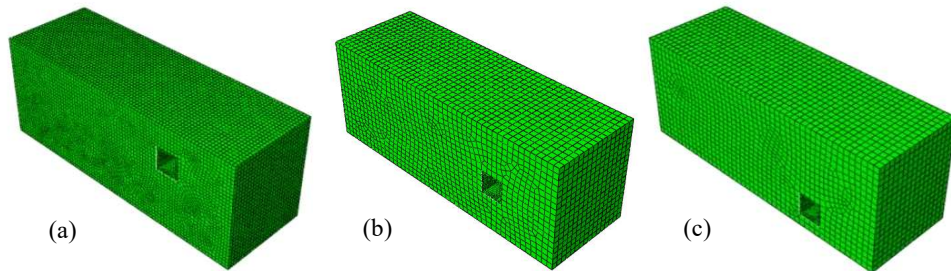
572

573

574

575

576

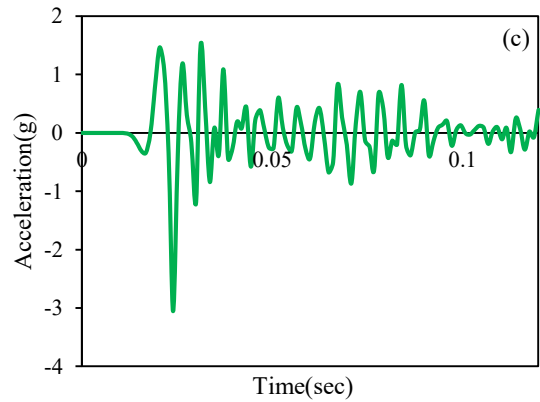
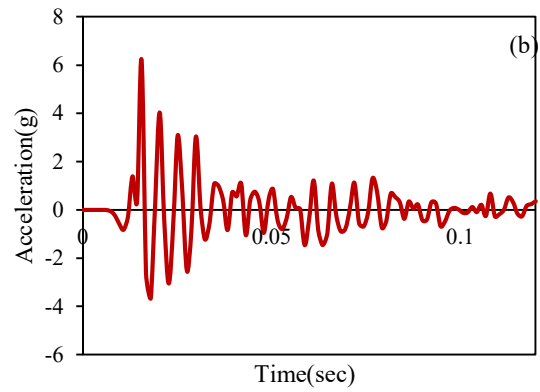
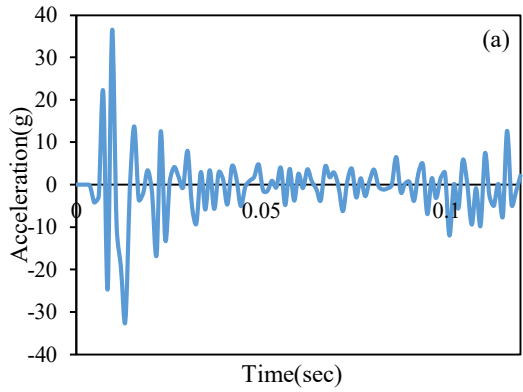


577

578

Fig 8. Tunnel at (a) 1 (b) 2 and (c) 3 m burial depth

579

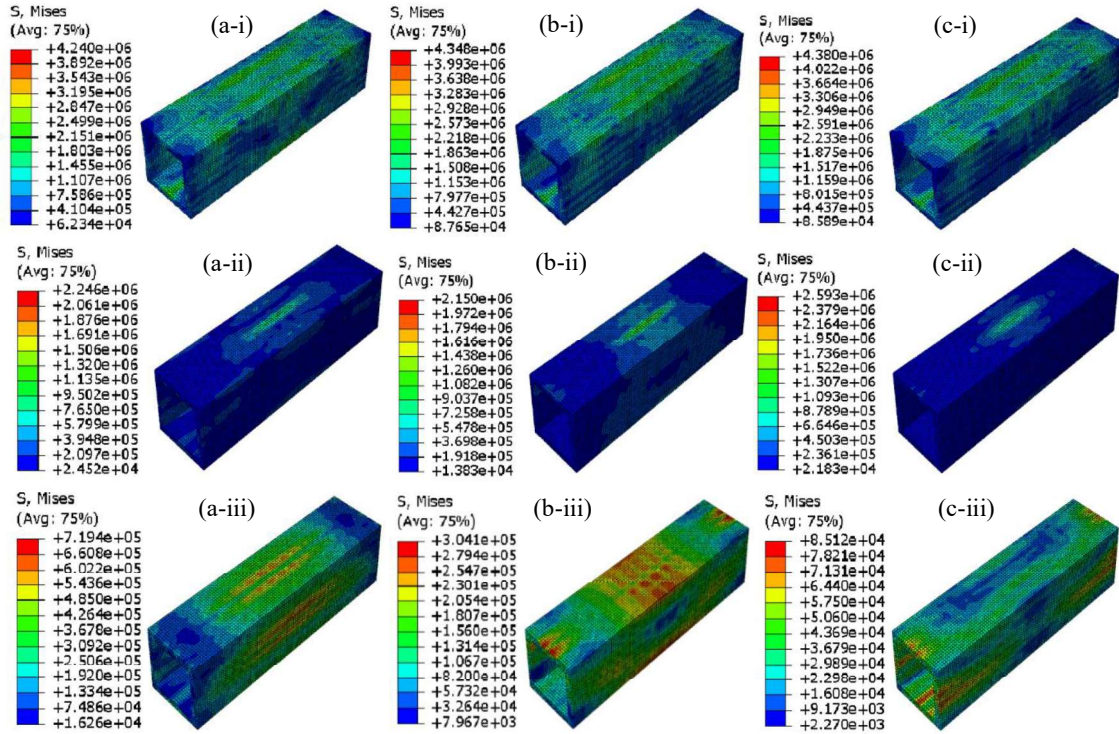


580

581
 582
 583
 584
 585
 586
 587
 588
 589
 590
 591
 592
 593
 594
 595
 596
 597
 598
 599
 600
 601
 602

Fig 9. Acceleration in tunnel having burial depth (a) 1 (b) 2 and (c) 3 m against surface blast loading

603



604

605

606

Fig 10. Mises stress in the tunnel front wall at (a) 0.024 (b) 0.036 and (c) 0.048 sec for surface blast loading at (i) 1 (ii) 2 and (iii) 3 m burial depth

607

608

609

610

611

612

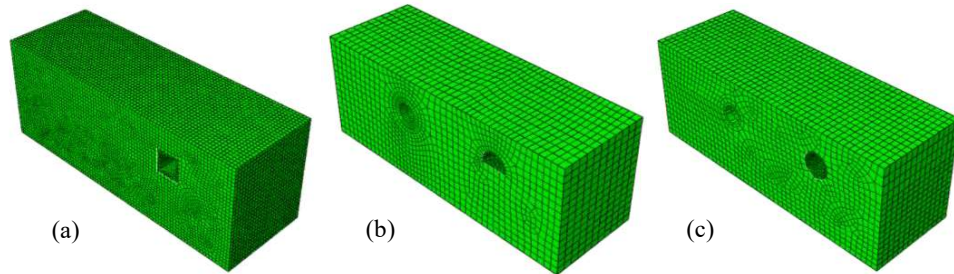
613

614

615

616

617



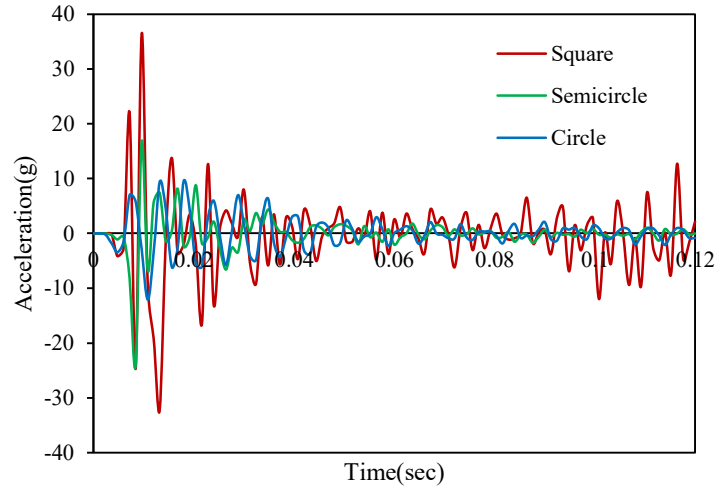
618

619

620

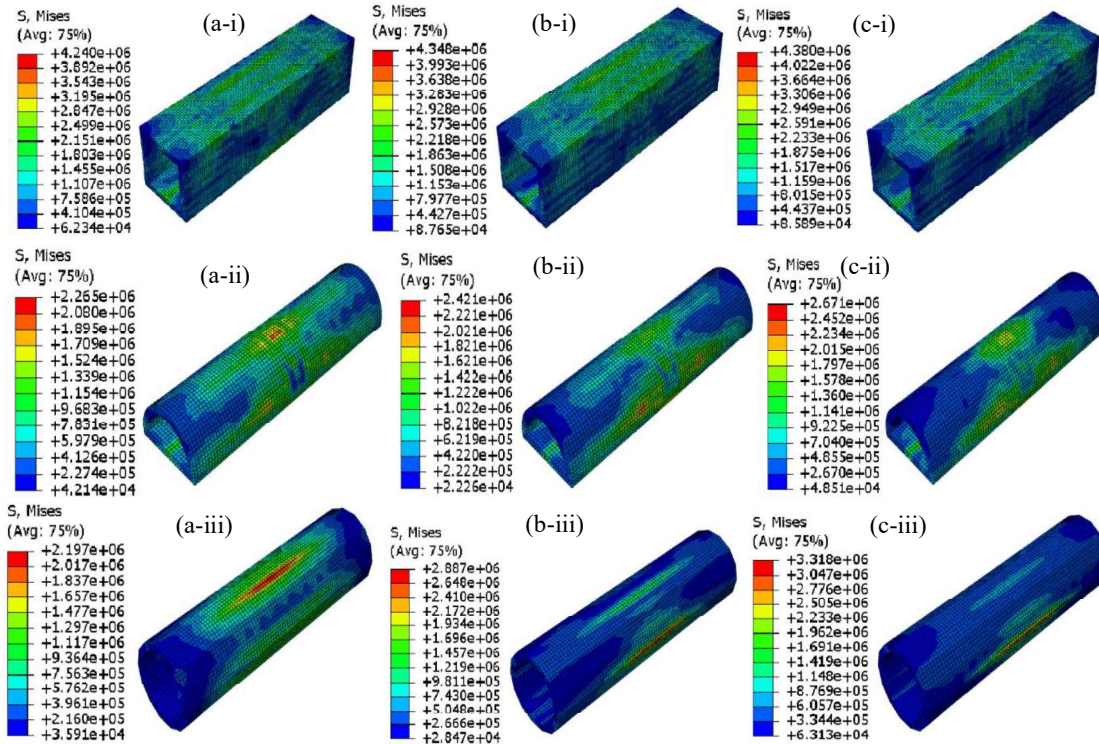
Fig 11. Tunnel with (a) square (b) semicircular and (c) circular shapes

621



622
623
624
625
626
627
628
629
630

Fig 12. Acceleration in tunnel having different tunnel shapes against surface blast loading



631
632
633
634
635

Fig 13. Mises stress in (i) square (ii) semicircular and (iii) circular tunnel against surface blast loading at (a) 0.024 (b) 0.036 and (c) 0.048 sec

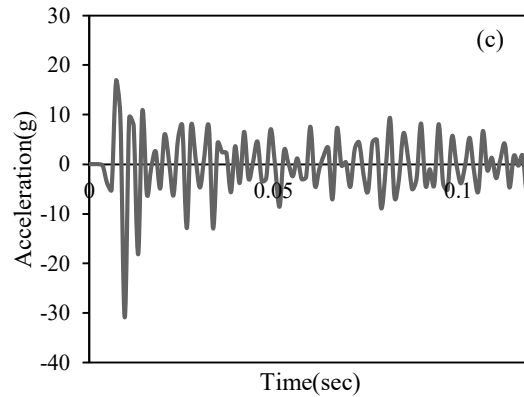
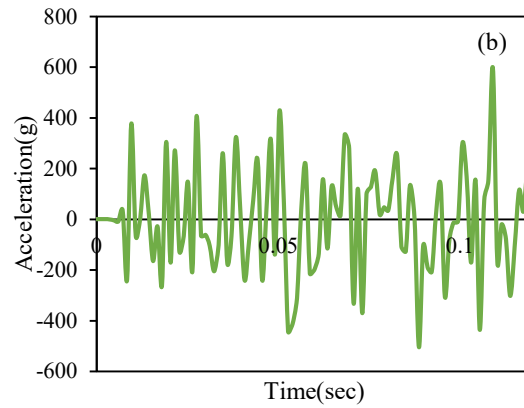
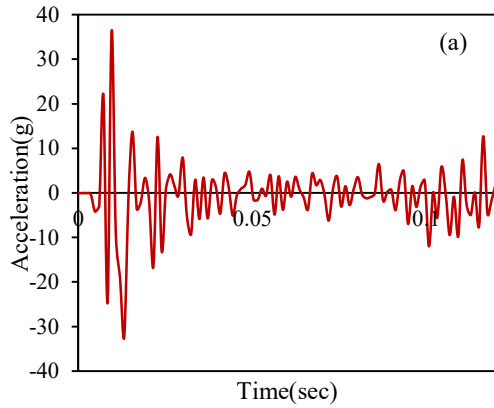
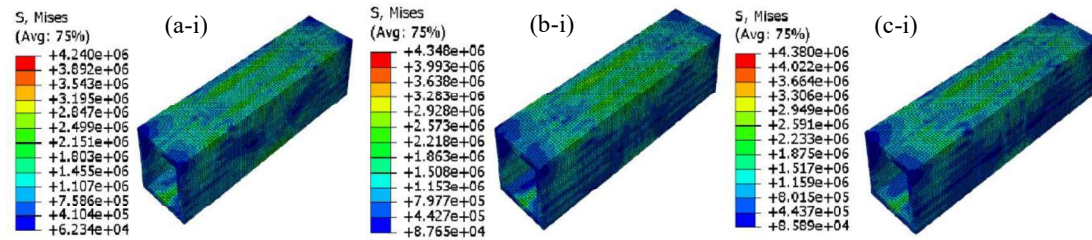


Fig 14. Acceleration in (a) reinforced cement concrete (b) plain cement concrete and (c) aluminum lining tunnels against surface blast loading

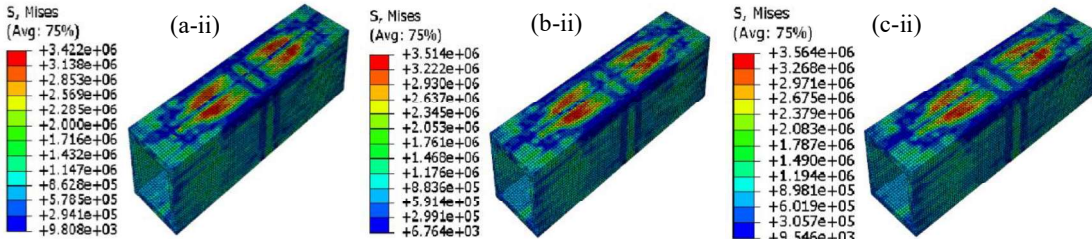
636

637
 638
 639
 640
 641
 642
 643
 644
 645
 646
 647
 648
 649
 650
 651
 652
 653
 654
 655
 656
 657

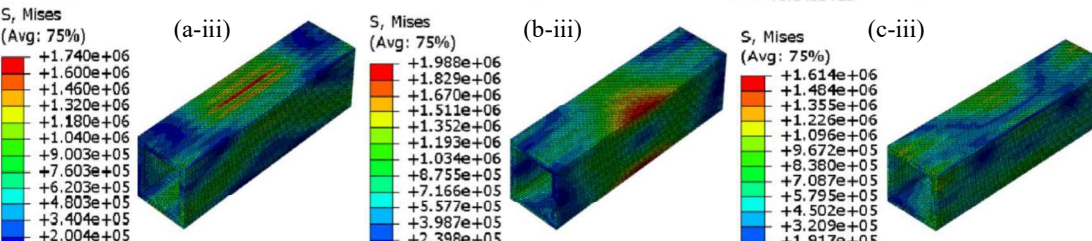
658



659



660



661 Fig 15. Mises stress in (i) RCC (ii) PC and (iii) Aluminum lining tunnels against surface blast
 662 loading at (a) 0.024 (b) 0.036 and (c) 0.048 sec
 663
 664
 665
 666
 667
 668
 669
 670
 671
 672
 673
 674
 675
 676
 677
 678
 679
 680

681

Table 1 Material constant for Aluminium and Steel

Description	Aluminium 2024 [Senthil et al. (2018)]	Weldox 460E [Borvik et al (2001)]
Density (kg/m ³)	2710	7850
Young's Modulus (N/mm ²)	71000	200000
Poisson's ratio	0.33	0.33
Yield stress constant A (N/mm ²)	265	490
Strain hardening constant B (N/mm ²)	426	807
n	0.34	0.73
Viscous effect C	0.015	0.0114
Thermal softening constant m	1	0.94
Reference strain rate ϵ_0	1	0.0005
Melting temperature (K)	893	1800
Transition temperature (K)	293	293
Fracture strain		
Constant	D ₁	0.13
	D ₂	0.13
	D ₃	-1.5
	D ₄	0.011
	D ₅	0
		0.0705
		1.732
		-0.54
		-0.015
		0

682

683

684

685

686

687

688

689

690

691

692

693

Table 2 Material constants for concrete material [Senthil et al. (2020)]

Description	Numerical Value
Density (kg/m ³)	2400
Young's Modulus (N/mm ²)	19700
Poisson's ratio	0.2
Dilation angle	35°
Eccentricity(m)	0.1
K	0.66
σ_{b0}/σ_{c0}	1.16

694

695

696

697

698

699

700

701

702

703

704
705
706

Table 3 Concrete compressive behavior [Senthil et al. (2020)]

Yield stress (N/mm ²)	Inelastic strain
20.0	0
19.8	0.00015
19.6	0.00025
19.4	0.00035
19.1	0.00045
18.8	0.00055
18.5	0.00065
18.1	0.00075
17.7	0.00085
17.4	0.00095
17.0	0.00105
16.6	0.00115
16.3	0.00125
15.9	0.00135
15.5	0.00145
15.2	0.00155
14.9	0.00165
14.5	0.00175
14.2	0.00185
13.9	0.00195
13.6	0.00205
13.3	0.00215
13.0	0.00225

707
708
709
710
711
712
713
714
715
716
717
718

Table 4 Concrete tensile behavior [Senthil et al. (2020)]

Yield stress (N/m ²)	Cracking strain
1.80	0
1.50	0.00012
0.60	0.00024
0.10	0.00065
0.05	0.00080

719
720
721
722
723
724

725

Table 5 Concrete compression damage [Senthil et al. (2020)]

Damage parameter d_c	Inelastic strain
0	0
0.006	0.00015
0.015	0.00025
0.027	0.00035
0.041	0.00045
0.057	0.00055
0.074	0.00065
0.092	0.00075
0.110	0.00085
0.129	0.00095
0.148	0.00105
0.166	0.00115
0.18	0.0012
0.20	0.0013
0.22	0.0014
0.23	0.0015
0.25	0.0016
0.27	0.0017
0.28	0.0018
0.30	0.0019
0.31	0.0020
0.33	0.0021
0.34	0.0022

726

727

728

729

730

731

Table 6 Concrete tensile damage [Senthil et al. (2020)]

Damage Parameter	Cracking Strain
0	0
0.40	0.00012
0.69	0.00024
0.92	0.00065

732

733

734

735

736

737

738

739

Table 7 Material constant for soil [Senthil et al. (2020)]

Density (kg/m^3)	Elastic modulus (N/mm^2)	Poisson ratio	Dilatation angle	Friction angle	Flow stress ratio
1850	29	0.36	1	31	0.778

740

741